Biomolecular Condensates of Functional Proteins: Mechanistic Insight of The Fibrillation Pathway

M.Sc. Thesis

By

Abhradip Mallik

Roll No. 2203131022

DEPARTMENT OF CHEMISTRY

INDIAN INSTITUTE OF TECHNOLOGY INDORE

May 2024

Biomolecular Condensates of Functional Proteins: Mechanistic Insight of The Fibrillation Pathway

A THESIS

Submitted in partial fulfillment of the
requirements for the award of the degree
of
Master of Science

by

Abhradip Mallik

DEPARTMENT OF CHEMISTRY
INDIAN INSTITUTE OF TECHNOLOGY INDORE

May 2024

Indian Institute of Technology Indore

DECLARATION

I hereby certify that the work which is being presented in the report entitled **Biomolecular Condensates of Functional Proteins: Mechanistic Insight of the Fibrillation Pathway** is an authentic record of my own work carried out during the time period from August 1, 2023 to May 2, 2024 under the supervision of Prof. Tushar Kanti Mukherjee.

Abhradip Mallik
17/5/24

Signature of the student
(Abhradip Mallik)

This is to certify that the above statement made by the candidate is correct to the best of my knowledge.

Signature of the Supervisor
(Prof. Tushar Kanti Mukherjee)

Acknowledgement

With great pleasure, I wish to express my sincere gratitude to my supervisor Prof. Tushar Kanti Mukherjee, for his able guidance and advice throughout this whole course. His enthusiasm and dedication have always inspired me. I am sincerely thankful to the Department of Chemistry and IIT Indore for providing me with the opportunity to pursue my M.Sc. project. I am grateful to Head of chemistry department, IIT Indore. I would like to extend my sincere thanks to my mentor Chinmaya Kumar Patel and to all my lab seniors. I extend my deep thanks to my lab mates, with their support and guidance. I was able to conduct my work smoothly and confidently.

Abhradip Mallik

Dedicated to my mother.

TABLE OF CONTENTS

List of Figures

Figure 6 (A) Effect of liquid phase and surface aging on the morphology of HSA. (B) Protein concentration determination inside the individual droplets using CLSM technique by comparing FL signal intensities between HSA (RBITC)+ PEG and HSA (RBITC) -PEG samples @ d1. (C) Size distribution histograms with time in liquid aging. (D, E) Protein concentration determination inside the individual droplets in surface aging by comparing the day wise samples FL signal intensities. (F) Size distribution histograms for surface aged samples. The data points represent the mean ± s.e.m. for three independent measurements for three (n = 3) independent experiments. All scale bars correspond to 5 μm

Figure 7 (A) Microscope images of d-1, d-7, d-14 were collected with Raman instrument set up to take spectra of individual droplets and fibril (B) Time-dependent individual Raman spectra (λ = 532 nm) of HSA+10% PEG of d-1, d-3, d-5, d-7 and d-14 on the glass slide. Spectra were normalized with Phenylalanine peak (red asterisk) at 1002 cm^{-1} for comparison. (C) Normalized Raman spectra of amide-I band of the HSA with the time. (D) FWHM (cm^{-1}) measurements of normalized amide I spectra of HSA+10% PEG with time (E) Tyrosine Fermi doublet (I_{850}/I_{830}) intensity comparison by bar diagram for the time-dependent HSA+10% PEG samples. (F) Microscope images were taken by Raman instrument set up for the surface dried samples at d-1 and d-7. (G) Time-dependent Raman spectra were recorded for the surface dried samples. Spectra were normalized at Phenylalanine peak (red asterisk) at 1002 cm^{-1} for comparison. (H) Normalized Raman spectra of amide-I band for d-1 and d-7 samples. (I), (J) represent the FWHM (cm^{-1}) measurement and Tyrosine Fermi doublet (I_{850}/I_{830}) intensity comparison for surface dried samples respectively.

Figure 8 (A) Confocal images of HSA 500 μM bound with 20 mM SDS, in presence of PEG 10% at day 1 to day 29. (B) Confocal images of HSA+10% PEG with $CuCl_2$ (250 μM) at day 1 to day 3 and Solid aggregates like structure formed @ d 3

Figure 9 (A) Turbidity assay of ligand bound HSA @d-1. (B) Changes in the CD spectra, (C) MRE_{222} profile, Samples were diluted by 100-fold before spectral measurements. (D) Deconvoluted FTIR spectra of ligand bound HSA incubation at 37 °C of d-1, the bar diagram represents the percentage of secondary structures alternation in ligand bound study estimated from the deconvoluted FTIR spectra. (E) Normalized Tryptophan FL intensity profile of HSA+10% PEG in presence of ligands.

Figure 10 Surface aging phenomena of $CuCl_2$ bound HSA of day 1, day 7 and day 14 samples. All scale bars correspond to 5 μm.

Figure 11 (A) Schematic representation of the procedure for phase separation study of HSA+ Tf in the same milieu under CLSM. (B) Time-dependent CLSM images of HSA+Tf in presence of 10% PEG by following the procedure (1). (C) CLSM images of HSA (fiber)+ Tf (droplets). (D) Surface aging CLSM images of HSA+Tf+ 10% PEG sample with time. Surace aged sample were incubated at 37 ºC. All scale bars correspond to 5 μm.

Abbreviation

mg	Milligram
Mol	Mole
g	Gram
mL	Millilitre
°C	Degree Celsius
%	Percentage
H	Hour
Min	Minute
μM	Micro molar
μm	Micro meter

Acronyms

ALS	Amyotrophic lateral sclerosis
HSA	Human serum albumin
CSF	Cerebro Spinal Fluid
LCD	Low complexity domain
LLPS	Liquid-Liquid phase separation
IDR	Intrinsically Disordered Region
BSA	Bovine Serum Albumin
PEG	Polyethylene Glycol
FESEM	Field Emission Scanning Electron Microscopy
AFM	Atomic Force Microscopy
FTIR	Fourier Transform Infrared
RBITC	Rhodamine B Isothiocyanate
CLSM	Confocal Laser Scanning Microscopy
ThT	Thioflavin T
SDS	Sodium Dodecyl Sulfate
Tf	Transferrin

Abstract

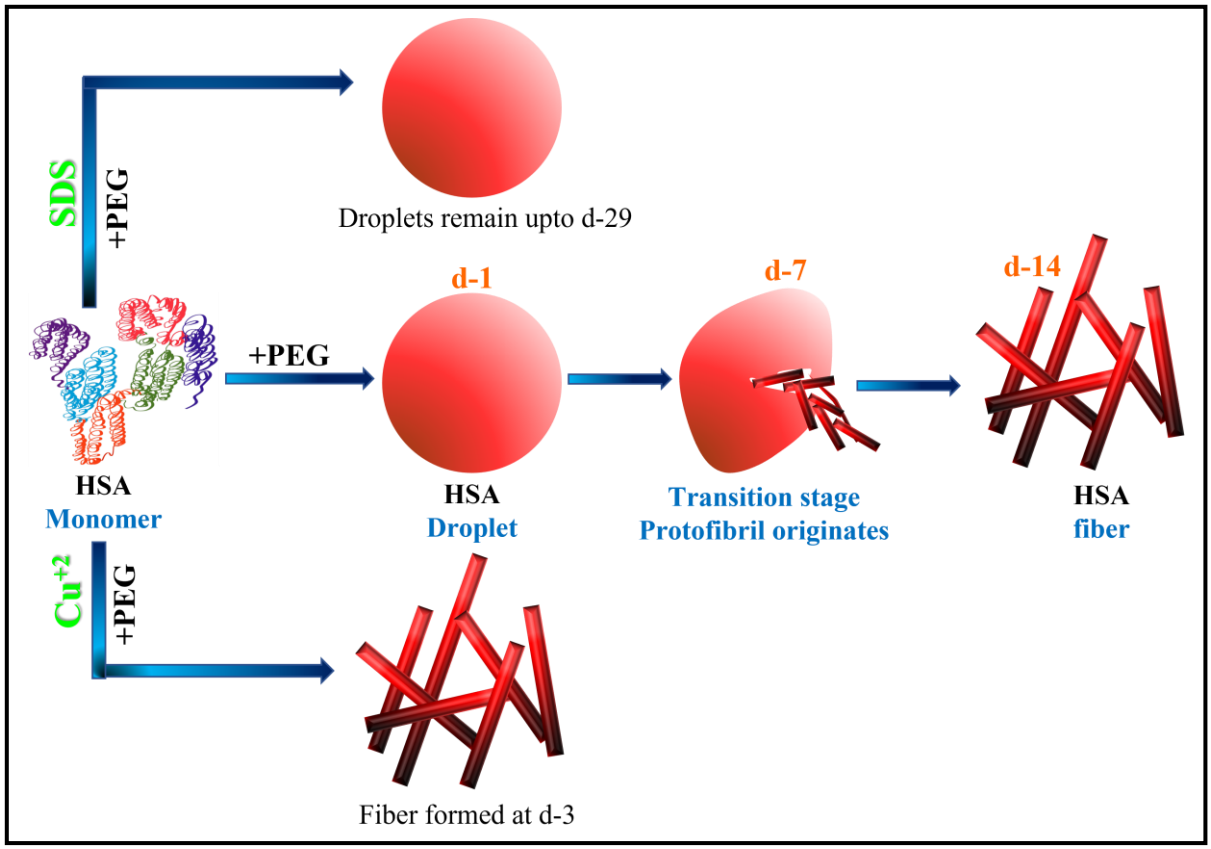

Protein aggregation or misfolding causes a variety of neurodegenerative diseases. Amyloid-beta peptide (Aβ) build-up in brain interstitial compartments causes degenerative neuropathies in Alzheimer's disease. This study explores the impact of Human Serum Albumin (HSA) on fibril development in cerebrospinal fluid (CSF) in the brain. So, HSA fibrillation has a significant role in amyloid plaque formation in CSF.The HSA fibrillation pathway is unknown. We investigate the fibrillation pathway and the modulatory effect of metal ions like Cu^{+2}, Fe+3, and surfactant like SDS through imaging and spectroscopic techniques. There were several studies on the fibrillation of prion like proteins and disordered proteins. However, there is a lack of knowledge about how an ordered protein undergoes fibrillization, such as the HSA. Numerous studies have delved into HSA fibrilization, yet a comprehensive comprehension of the fibrillization pathway and the impact of metal ions and surfactants remains necessary. However, we observed that HSA globular protein without IDRs and LCDs enhances LLPS via enthalpy and promotes fibril formation from the liquid like protein condensates. Eventually, this study will include the phase separation behaviour of the holo-Transferrin (h-Tf) and HSA upon macromolecular crowding in the milieu. The study explores the intriguing behaviour of h-Tf droplets and HSA droplets in fibrillization.

Chapter 1

Introduction

1.1. Introduction

Protein aggregation or misfolding is a significant contributing factor in the development of several human clinical disorders, including amyloidosis. These conditions encompass Amyotrophic lateral sclerosis (ALS; affects the motor neurons), neurodegenerative diseases, prion diseases, and type II diabetes [1]. Alzheimer's disease is a degenerative neuropathies disorder defined by the deposition of amyloid-beta peptide (Aβ) in the interstitial compartments of the brain [2]. As people become older, a greater proportion get Alzheimer's dementia. Alzheimer's dementia affects 5% of adults aged 65 to 74, 13.1% of those aged 75 to 84, and 33.3% of people aged 85 and above [3]. The present study investigates the influence of HSA on the proliferation of fibrils generated by both Aβ (1– 40) and Aβ (1– 42). The quantity of amyloid fibers produced is directly associated with the ratio of unbound Aβ to albumin, without any competitive binding. The observations indicate that HSA significantly contributes to regulating the formation of Aβ fibrils in the brain interstitium [4]. Currently, there is a lack of mechanistic understanding regarding the process by which HSA progresses to the fibrillation stage. (Protein oligomers to amyloid structure). The objective of our study is to (i) investigate the process of protein fibrillation (ii) why the liquid-to-solid transition is faster in liquid aging? (iii) modulatory effect of ligands in the transition and (iv) find the intermediate stage using an in vitro approach. Because once the insoluble amyloid fibril is formed it is impossible to back to oligomer stage, so if we have a transparent idea on the fibrillation pathway of HSA then it will contribute some impact on the Alzheimer's disease related research [5]. Samir K. Maji and Hyman group previously reported on α-Synuclein and Tau protein those proteins are related to Parkinson's and Alzheimer's disease respectively [11, 24]. So, to prevent or prolong the fibrillation stage Specifically, we intend to replicate the physiological conditions found in vivo in order to either inhibit or prolong the fibrillation stage by the effect of various ligands. Various studies have been already explored for HSA fibrilization but it is utmost important to explore a detailed study of the pathway of fibrillization along with the effect of external parameters like metal ion and surfactant.

Aggregation of proteins, in general, is the results from the unnatural aggregation of inherently disordered or misfolded proteins and may be divided into three structural classes: amorphous aggregates, oligomers, and amyloid fibrils [6]. The highly structured, insoluble, and fibrillar deposition of amyloid aggregates which can develop from naturally folded proteins or

from intrinsically disordered proteins and become the basis for a number of neurodegenerative disorders. The construction of amyloid fibrils is related with a number of sequential associations, such as β-strands being stacked into β-sheets and it interacting with each other to create protofilaments and protofilaments stacking on or twisting around one another to form a fibril. Many factors contribute to the stability of these various protein aggregates, including hydrogen bonding between the backbone amides, van der Waals interaction between the interface of the side chains, hydrophobic interaction initiated from the hydrophobic pockets in the amino acids, electrostatic interaction, and so on [7].

Numerous proteins associated with diseases exhibit intrinsically disordered regions (IDRs) that contain low-complexity domains (LCDs) within their amino acid sequence, undergo liquid-liquid phase separation (LLPS) without inert macromolecular crowders. [8]. While the involvement of inert crowders in the LLPS of proteins containing IDRs is well known, the effect of macromolecular crowding on the physicochemical characteristics of globular proteins has received less attention. But our group have showed that HSA globular protein without IDRs and LCDs in their amino acid sequence drive towards LLPS and the primary mechanism behind LLPS of HSA is enthalpically regulated hydrophobic contacts involving aromatic and/or nonaromatic residues [9]. LLPS is a spontaneous process that occurs in aqueous mixture of proteins, RNA, polypeptides, polymers, and/or polyelectrolytes. It produces membrane-free liquid-like condensates through multivalent intermolecular interactions. The volume exclusion effect, which often favours a compact native state because to steric repulsions, has been effectively used to explain protein-protein and protein-crowder interactions. The existence of inert crowders reduces the amount of space available for the proteins, which leads to the steric repulsions between crowders and proteins. The major type of this non-specific steric impact is entropic [10]. The process by which supramolecular nanofibrils are created from uniform solutions of amino acids and short peptides involves the production of concentrated liquid droplets by a LLPS mechanism. These droplets subsequently undergo a thermodynamically favourable transformation into fibrils. [11]. Liquid-like droplets change to a solid gel-like fibers [9]. Liquid droplets or coacervates or condensates possess some common characteristics (i) highly mobile in nature (ii) Spherical in shape but deform in physical contact (iii) fuse and eventually revert back to spherical shape, (iv) show Ostwald ripening, (v) liquid droplets are temperature and pH dependent etc [11].

HSA (Human Serum Albumin) and BSA (Bovine Serum Albumin) are both globular proteins and both have analogous functions as well as similar physicochemical properties.

However, BSA is more accessible, that is why it is employed in many scientific investigations instead of HSA, and the outcomes are then applied to HSA. The HSA protein consists of a total of 585 amino acids, in contrast to BSA which is composed of 583 amino acids. The modest variations in their sequence contribute to the observation that HSA and BSA exhibit a sequence identity of just 75.8%. Additionally, both proteins possess a similar molecular weight of roughly 66,430.3 Da [3],[12].

In order to identify the phase transition state in invitro conditions while maintaining physiochemical conditions. Now, we are interested in the time dependent analysis HSA within an environment containing 10% PEG (pH 7.4 Phosphate buffer saline at physiological temperature, 37ºC) using Confocal microscope, FESEM, AFM, Fluorescence Spectrometer, CD Spectroscopy, UV-vis Spectrometer, Rheometer and Fourier transform infrared (FTIR) spectroscopy technique. Our study involves phase separation of protein upon macromolecular crowding and effect of different metal ions and surfactant on the LLPS of HSA.

1.2. Scope of The Project

Soluble monomeric protein of HSA (Liquid)

Insoluble protein solid-like aggregates

Scheme 1. Transition of soluble monomeric form to insoluble fiber stage.

Many soluble functional proteins undergo fibrillization and causes various neurodegenerative diseases like Alzheimer's and Parkinson disease. HSA is one of the most abundant functional protein in human and its low concentration in CSF facilitates the amyloid plaque formation. The amyloid plaque is one of the leading causes of Alzheimer's disease.

Therefore, our objectives are to investigate:

1. How soluble monomeric functional protein, HSA undergo aggregation to give insoluble fibrillar aggregates?
2. Mechanistic insight and kinetic intermediates during liquid to solid phase transition.
3. How external parameters (metal ion, surfactant) affect the liquid to solid transition of HSA?
4. Why the fibrillization step is faster in liquid phase aging?
5. Reason behind fibrillization of HSA.
6. Liquid phase and surface aging phenomena of Transferrin and HSA in presence of crowder in the same milieu.

Chapter 2

Results and Discussion

2. Result and Discussion

The main soluble protein component of the circulatory system, serum albumins serve a variety of physiological purposes. The ability of this class of proteins to act as transporters for many substances is perhaps their most significant characteristic. BSA has undergone some of the most in-depth research within this class of proteins, in part due to the structural similarities between BSA (isolated from cow) and human serum albumin (HSA) [13]. Both albumins have identical binding sites on subdomains IIA and IIIA, and they both have a 76% sequence homology. The amino acids lining the binding sites are primarily hydrophobic [14]. HSA is composed of a solitary polypeptide chain, with a molecular weight of approximately 66 kDa and including around 585 amino acids.

2.1. Analysis of LCD, IDR and liquid to solid transition of HSA

The HSA molecule is structured into three homologous domains (I, II, III), which are further subdivided into nine loops (L1-L9) through the presence of 17 disulfide linkages. [15]. (**Figure 1. A)** shows the three-dimensional structure of HSA (The Crystal Structure of HSA (PDB Entry 7DJN; obtained from protein data bank). A number of proteins having low-complexity domains (LCDs) in their amino acid sequence and intrinsically disordered regions (IDRs) have recently been found to conduct LLPS in the presence or absence of inert macromolecular crowders [16]. To examine the presence of LCD and IDRs, the Simple Modular Architecture Research was employed in our study. Tool (SMART) and IUPred2 sequence prediction algorithms. SMART analysis of HSA predicted that HSA has no LCD regions and the IUPred2 algorithm revealed no disordered regions in HSA amino acid sequence (**Figure 1. B**). In this research, we have looked at the morphological alteration of HSA in the absence/ presence of polymeric crowder Polyethylene glycol 8 kDa (10 % PEG 8000 Da). The solution of 500 μM HSA was prepared in Phosphate buffer (PBS; pH 7.4) in the presence of 10% PEG. In time dependent daylight photographs **(Figure 1. C)** of the solution shows that the gradual increase in turbidity with time which directly corelate with the phase separation (Turbidity plot **(Figure 1. D)** was done by the equation ($\%T=100-100\times10^{-\text{Abs. maxima}}$) and solid-gel formed at day 14. Furthermore, strain-sweep experiment studies were performed to understand the mechanical behavior and viscoelastic properties between @d11 and @d14 of HSA+ 10% PEG. The strain-sweep rheological study showed that the values of the elastic storage modulus G′ (Surface elasticity) were significantly higher than the loss modulus G″

(Surface viscosity) up to a strain of 600% and 120% for @d14 and @d11 samples respectively, that suggesting the dominance of solid-like elastic behavior increases over the time. However, G″ dominated over G′ beyond a strain of 600% and 120%, indicating the conversion of gel to sol state beyond 600% and 120% for the sample d14 and d11 respectively.

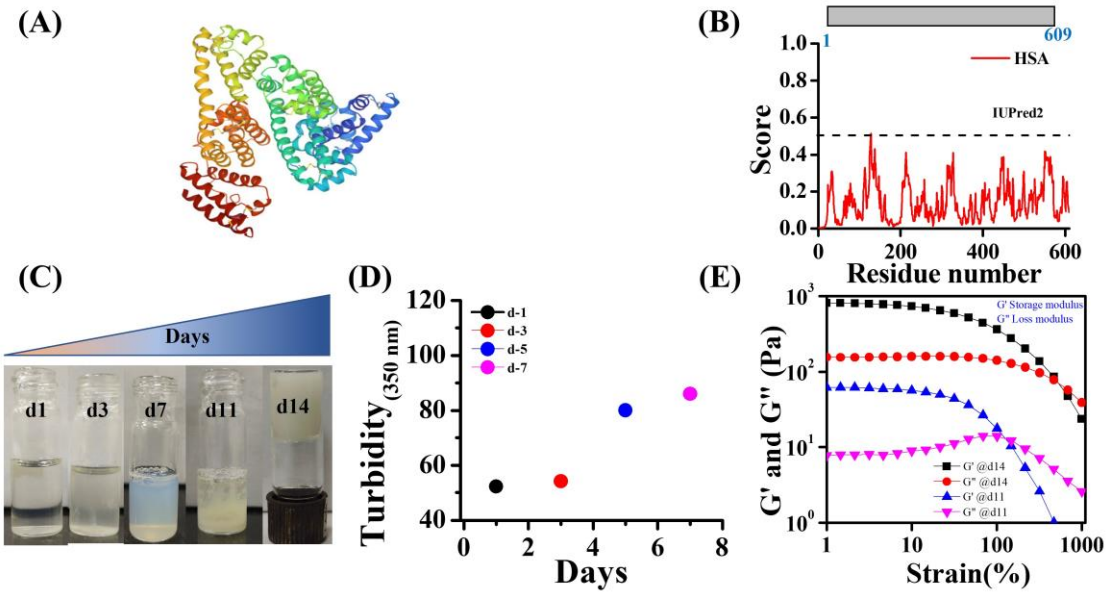

Figure 1. (A) The Crystal structure of HSA (PDB entry 7DJN) acquired from the Protein Data Bank.; (B) SMART and IUPred2 analysis of protein HSA (UniProt Id P02768); (C) Day wise images of HSA 500 μM+ 10% PEG ;(D) Turbidity assay of 500 μM HSA+10% PEG. (E) The time-dependent strain-sweep study in Rheometer of HSA+10% PEG of d11 and d14 showing the gel-strength increases with time.

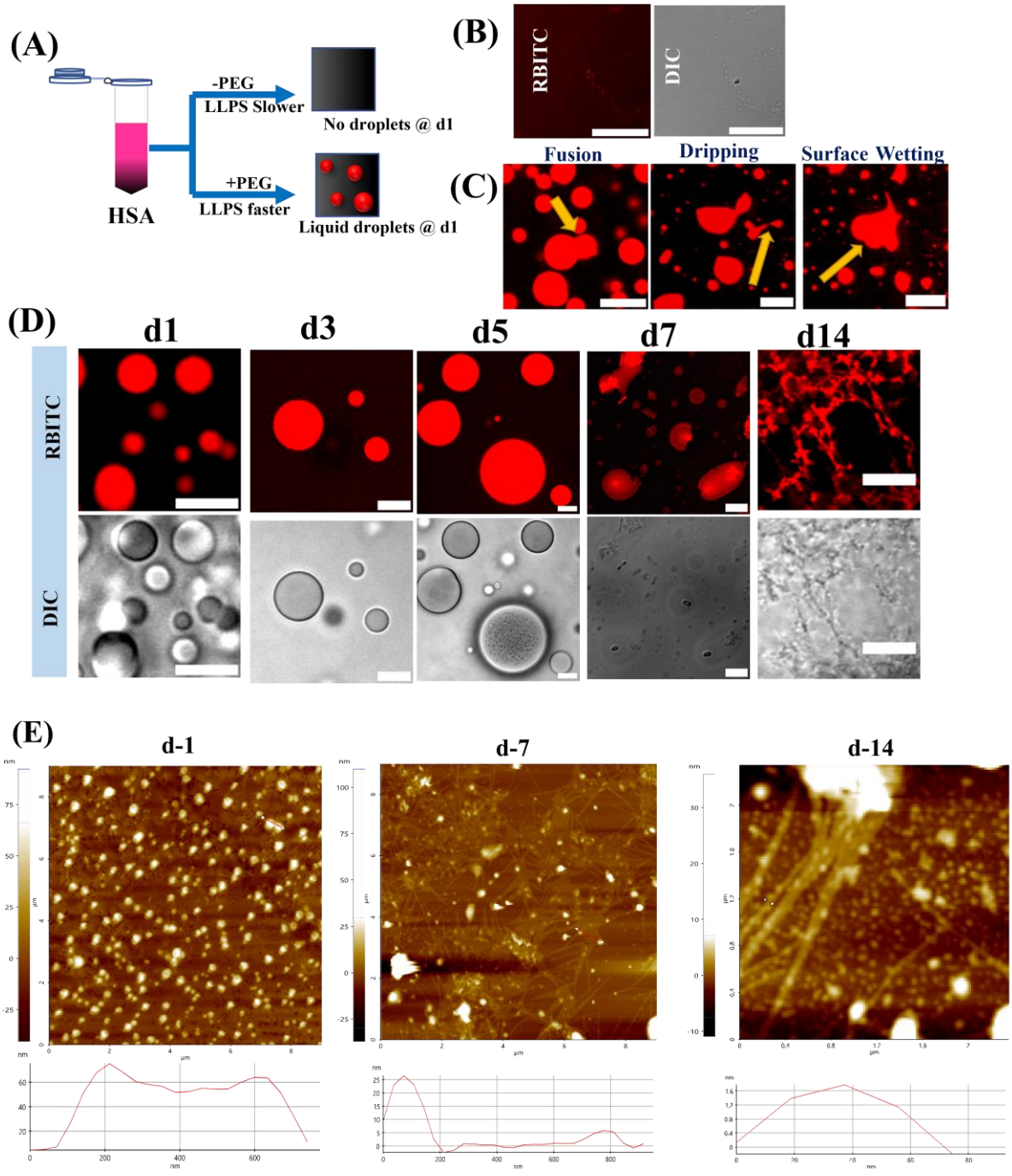

Figure 2. (A) Schematic representation of the influence of crowding in LLPS (B) CLSM images of HSA without PEG, reveals no droplets @ day 1. (C) Images captured using confocal microscopy reveal the fusion, surface wetting, and dripping behaviour of HSA droplets. These occurrences are highlighted with yellow arrows. (D) Time dependent study of CLSM images of 500 μM HSA+10% PEG in PBS; pH 7.4 (All scale bars of CLSM images are 5 μm). (E) AFM images also reveal the transition of droplet to fiber, with the decreasing in height from droplet to fiber. AFM images were recorded in tapping mode.

2.2. LLPS of HSA upon inert crowder and the morphology of droplets with time:

The essential protein concentration needed for LLPS has recently been found to be lowered and faster by the use of inert synthetic/protein crowders (**Figure 2. A**), which have been proven to effectively change the intermolecular protein interactions. [5],[11]. To replicate the phenomenon of intracellular crowding, we examined the behavior of Human Serum Albumin (HSA) in its distinct phase under two conditions: without any crowders, and in the presence of an inert synthetic crowder known as polyethylene glycol (PEG 8000 Da). Rhodamine B isothiocyanate (RBITC) tagged HSA at a concentration of 500 μM was used for phase behavior investigations under a confocal laser scanning microscope (CLSM). Day-to-day monitoring with CLSM demonstrates that droplet size grows day by day, with the intermediate stage of fiber development (droplets breaking and fibers emerging from the droplets) reached at day-7 and only fibers seen by day-14 (**Figure 2. D**). The uniform fluorescence signals emanate solely from within these assemblies, indicating the presence of RBITC-labelled HSA. However, when PEG 8kDa is not present, HSA exhibits no distinguishing characteristics in either the phase contrast or fluorescence images (**Figure 2. B**). The observed spherical assemblies have distinctive liquid-like characteristics, including spontaneous fusion, surface wetting, and dripping. These observations imply that these assemblies can be classified as liquid-like coacervates of HSA (**Figure 2. C**). Furthermore, in order to visualize the nanoscale morphology of the droplets and fibrils, we performed atomic force microscopy (AFM). For the preparation of AFM imaging, we have to dilute the protein-crowder sample around 200 times for better visualization in the microscope. In the liquid to solid transition steps, the droplet height decreased gradually with time **(Figure 2. E)**. @d-1 the height of the droplets around 50 nm to 60 nm, @d-7 the transition began i.e., the droplets ruptured and protofibril like structure originated. So, the height decreased to ~25 nm and at last @d-14 the height was ~1.5 nm for solid-like fibers.

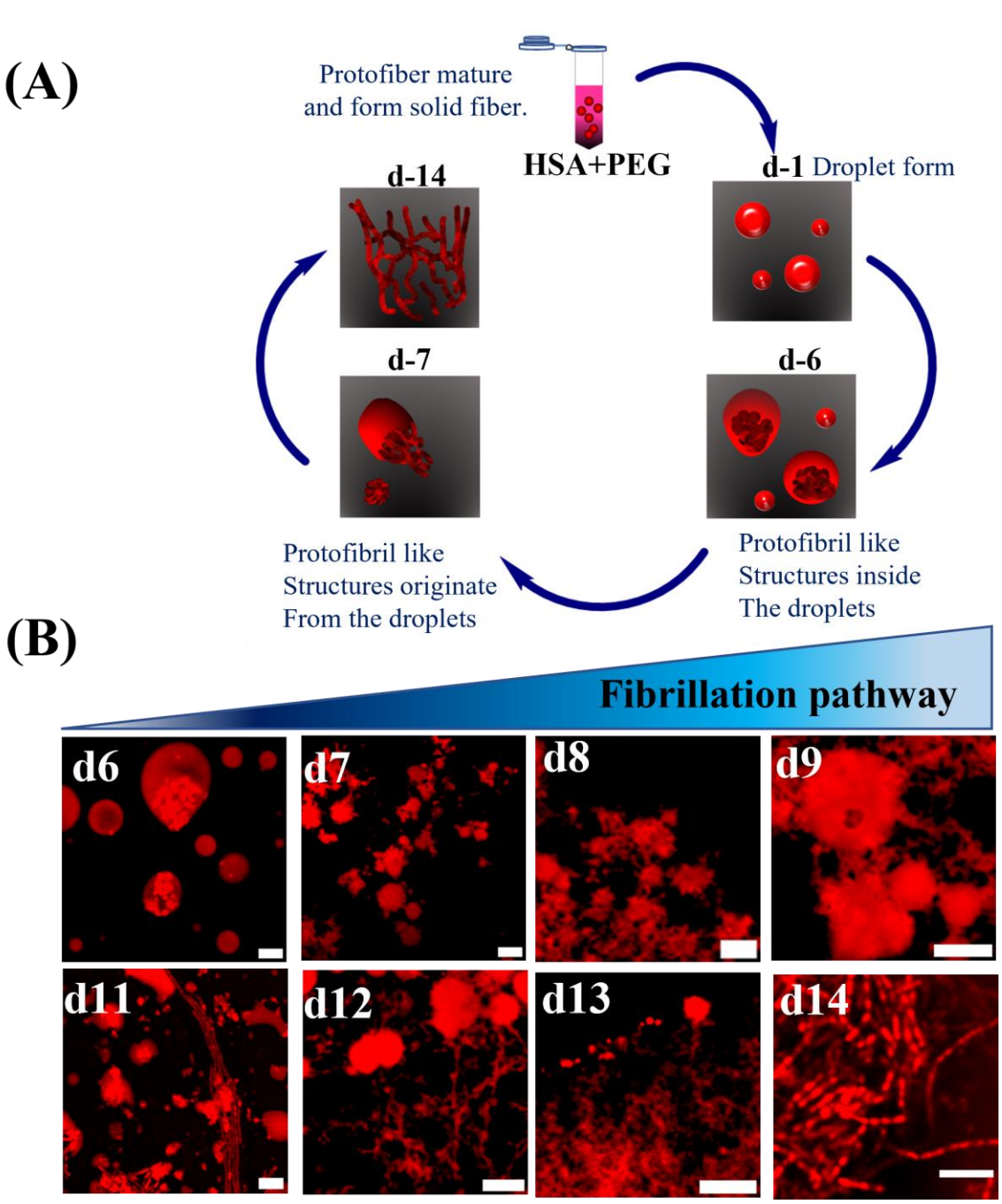

Figure 3. (A) Schematic representation of alternation of morphology of HSA droplets, in the transition stages of the fibrillation pathway. (B) CLSM images of transition stages of @ d6 to @d14. (All scale bars correspond to 5 μm).

2.3. Mechanistic insight of the fibrillation: analysis by CLSM, FTIR and CD-spectroscopy

Protofibrils and oligomers are metastable peptide assemblies observed during the growth of amyloid fibrils by a number of peptides, including the Alzheimer's amyloid plaque peptide Aβ [25]. These protofibrils persist for days when incubated in PBS at 37°C, with a slow transition to fibrillar structures apparent only after several days. In our day-wise study of alternation of droplet to fiber stage, there were several stages seen of transition to protofiber to mature fiber. These mechanistic insight of fibrillation studies have been not broadly discussed earlier for HSA fibrillation. We observed at day 6, small aggregation like structures was seen inside the droplets by CLSM (**Figure 3. B**) and gradually with passage of time droplets ruptured and protofibers originated from it. These protofibers were connecting together to form mature fiber at day 14 (**Figure 3. B**). The schematic representation (**Figure 3. A**) shows at a glance that how these fibrillations occur.

Furthermore, we were more curious to study the alternation of the secondary structures in the fibrillation pathway. There was a major role of β-sheet structure in the amyloid formation that facilitated the protofiber to fiber alternation. The native HSA consists of mainly α-helix (~67% α-helix and 18% β-sheet respectively) [16],[17]. Using deconvoluted FTIR analysis of 500 μM HSA and 10% PEG (in pH 7.4) sample, we observed that, the % of α-helix decreased along with the increased of that the β- sheet structures as a function of incubation time in 37ºC (from day 1 to day 14). β-sheets make up a larger fraction of the protein structure at the fiber stage (**Figure 4. A, B**). Probably, this factor could play a major role in HSA fibrillation. Eventually, we monitored the secondary structure of HSA with the function of incubation time using far-ultraviolet circular dichroism (CD) measurements. Important to note that here we diluted our 500 μM+ 10% PEG by 100 times to avoid the HT voltage saturation. The droplets remain unaltered as revealed from the AFM images (we diluted to record AFM images ~200 times). HSA inside the droplet exhibits two characteristic minima at 208 and 222 nm, signifying α-helix rich secondary structures. The time-dependent CD spectra reveals significant alteration in the secondary structure of HSA during droplet to fiber formation. **(Figure 4.C)**. The calculated MRE_{222} values reveal that ellipticity at 222 upon incubation time decreases (negative value decreases) gradually and saturates upon incubation for 14 days. **(Figure 4. D).** The decrease in helicity was for the concomitant gain in β-sheet rich structures [8]. So, from the deconvoluted FTIR data and CD-measurements revealed that during aging of HSA+10% PEG, the alternation of secondary structures had been occurring, that led the fibrillation pathway of HSA.

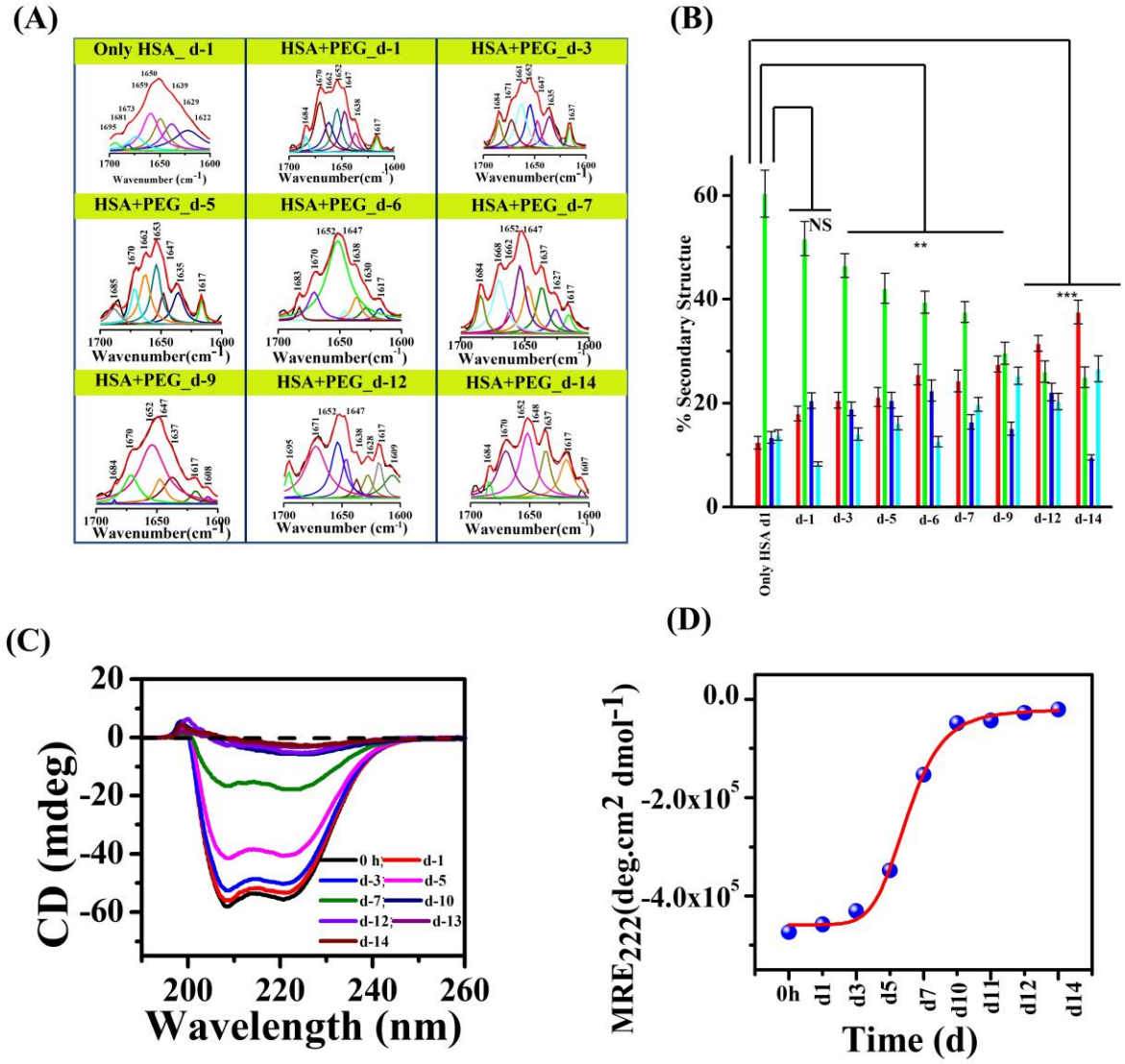

Figure 4. (A) Deconvoluted FTIR spectra of 500 μM HSA+10% PEG at 37 °C in time-dependent manner (B) The bar diagram represents, the percentage of secondary structures alternation of HSA+10% PEG from the deconvoluted FTIR spectra. The data points represent the mean ± s.e.m. for three independent measurements for three (n = 3) independent experiments. Statistical significance was assessed by a two-tailed, unpaired Student's *t*-test with ***, *P* value < 0.001; **, *P* value < 0.01; and not significant (NS), *P* > 0.05. (C) Changes in the CD spectra, (D) MRE_{222} profile, Samples were diluted by 100-fold before spectral measurements.

2.4. ThT FL and Trp FL assay: Infer secondary and conformational structural changes

Amyloids (protein fiber) are generally β-sheet enrich structure. To identify the interfaces that are rich in β-sheets, a Thioflavin T (ThT) binding experiment was conducted. Upon attaching to amyloid fibrils, the benzothiazole dye Thioflavin T exhibits increased fluorescence. while bound to different amyloid fibrils, ThT exhibits a remarkable fluorescence amplification compared to its extremely weak fluorescence while in water. ThT has been utilized as a specific marker for the detection of amyloid fibrils. for this reason, ThT shows a negligible fluorescence intensity upon binding with HSA alone [9]. Nevertheless, the intensity exhibits a progressive rise when HSA droplets are present during the incubation period. This observation provides compelling evidence that the decrease in helicity of HSA within the droplets is counterbalanced by a simultaneous increase in intermolecular contacts rich in β-sheet structures (**Figure 5. A**). We have also performed, the ThT bound CLSM study, that revealed the ThT FL intensity increases with fibrillar growth **(Figure 5.C).** The protein, HSA also have intrinsic blue fluorescence **(Figure 5. D)** but the intensity was too low compare to ThT bound protein of @d-14 sample **(Figure 5. E).** The intensity was measured in 'image j' and the CLSM images were taken by maintaining the same intensity and focal length of the instrument.

In order to investigate the structural alterations linked to the phase transitions of HSA, it is necessary to conduct a comprehensive analysis. The fluorescence intensity of a fluorophore is influenced by its surrounding environment, indicating that alterations in the tryptophan (Trp) fluorescence intensity may be associated with modifications in the conformation of the protein. An elevation in intensity **(Figure 5.B)** is noted, and the intensity was not so enhanced in only HSA protein solution. This indicate that the conformational changes occur faster rate in presence of crowders. A minimal red shift of around 2-3 nm in the emission maximum with time is noticed. The observed augmentation in the fluorescence intensity indicates a potential reorganization of neighbouring residues in the vicinity of the Trp. Conversely, alterations in the emission peak indicate a comparable polar milieu or solvent exposure surrounding the Trp. This observation is supported by measurements that were conducted with a time-resolved approach [19].

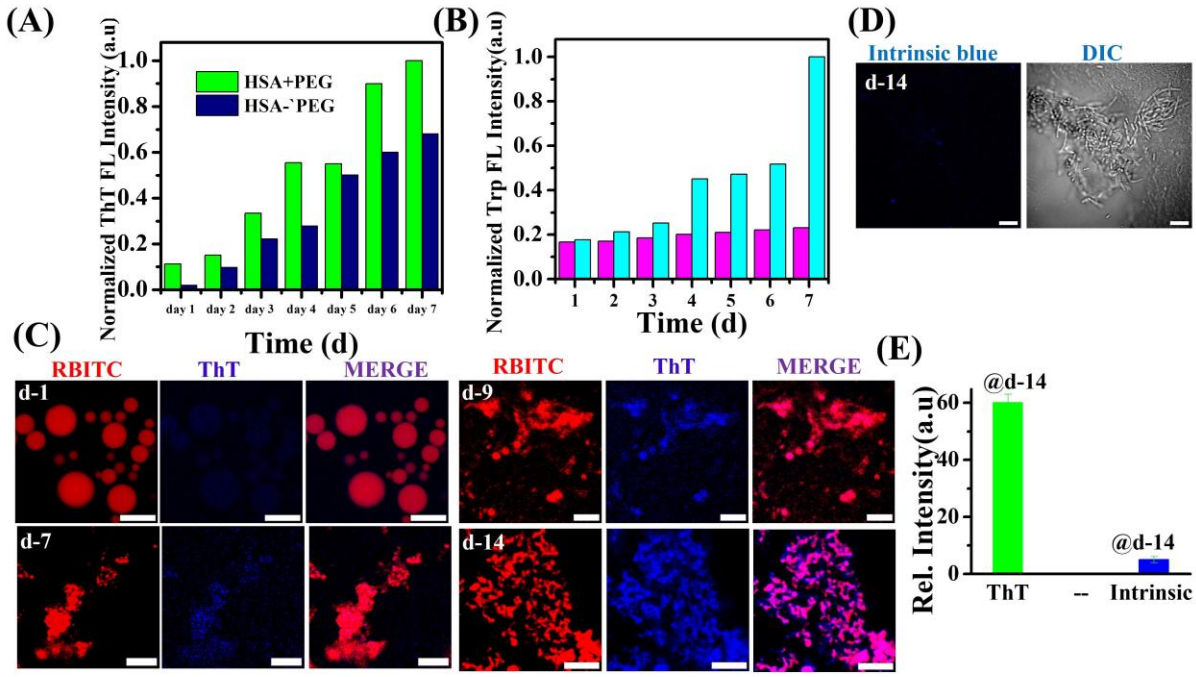

Figure 5. (A) Normalized ThT FL intensity assay; ThT (20 μM) with the function of incubation time (day 1 to day 7) of HSA 500 μM+ 10% PEG in PBS (pH 7.4); ($\lambda_{excitation}$ = 450 nm and $\lambda_{emission}$ in the range of 490-550nm). (B) Aggregation is facilitated by conformational changes in HSA within condensates. HSA tryptophan fluorescence spectra from the first to the seventh day of incubation with 10% PEG-8kD; 280 nm was the excitation wavelength and maximum absorbance at 340 nm. (C) Time-dependent CLSM images of ThT bound HSA. (D) Intrinsic blue fluorescence of HSA @d-14 (fiber). (E) Bar diagram shows the blue FL intensity comparison of ThT bound and intrinsic blue FL of the sample @d-14.

2.5. Morphological changes of droplets in liquid phase vs surface aging with time

Interestingly, we observed that the fibrillation process took place in liquid aging manner but when we surface aged the sample (HSA-RBITC labelled + PEG 10%) after 4-5 hours of incubation at 37 ºC, the droplets had been sustained over the period day 14 **(Figure 6. A).** The probable reason was in surface aging manner that there was no simultaneous fusion, coalescence that's why effective protein concentration was not increasing over a long time period but that was not in the case in liquid aging. We approximate determined the protein concentration inside the droplets by CLSM technique and we approximately estimated that inside the droplets the protein concentration was increased by around 10 times than the disperse phase by measuring intensity in 'Image j **(Figure 6. B, C)** The technique is widely reported [7]. From the size distribution profile, we showed that along with increasing the protein

concentration, the size of droplets increases due to fusion (@d1 the average mean size of the droplet ~3.6 μm and @d5 ~ 6.2 μm). In contrast, when we measured the approximate protein concentration by comparing intensity, the protein concentration almost same of the @d-1, @d-7 and @d-14 samples **(Figure 6.D, E)** and the size of the droplets remain unchanged with time **(Figure 6. F)**.

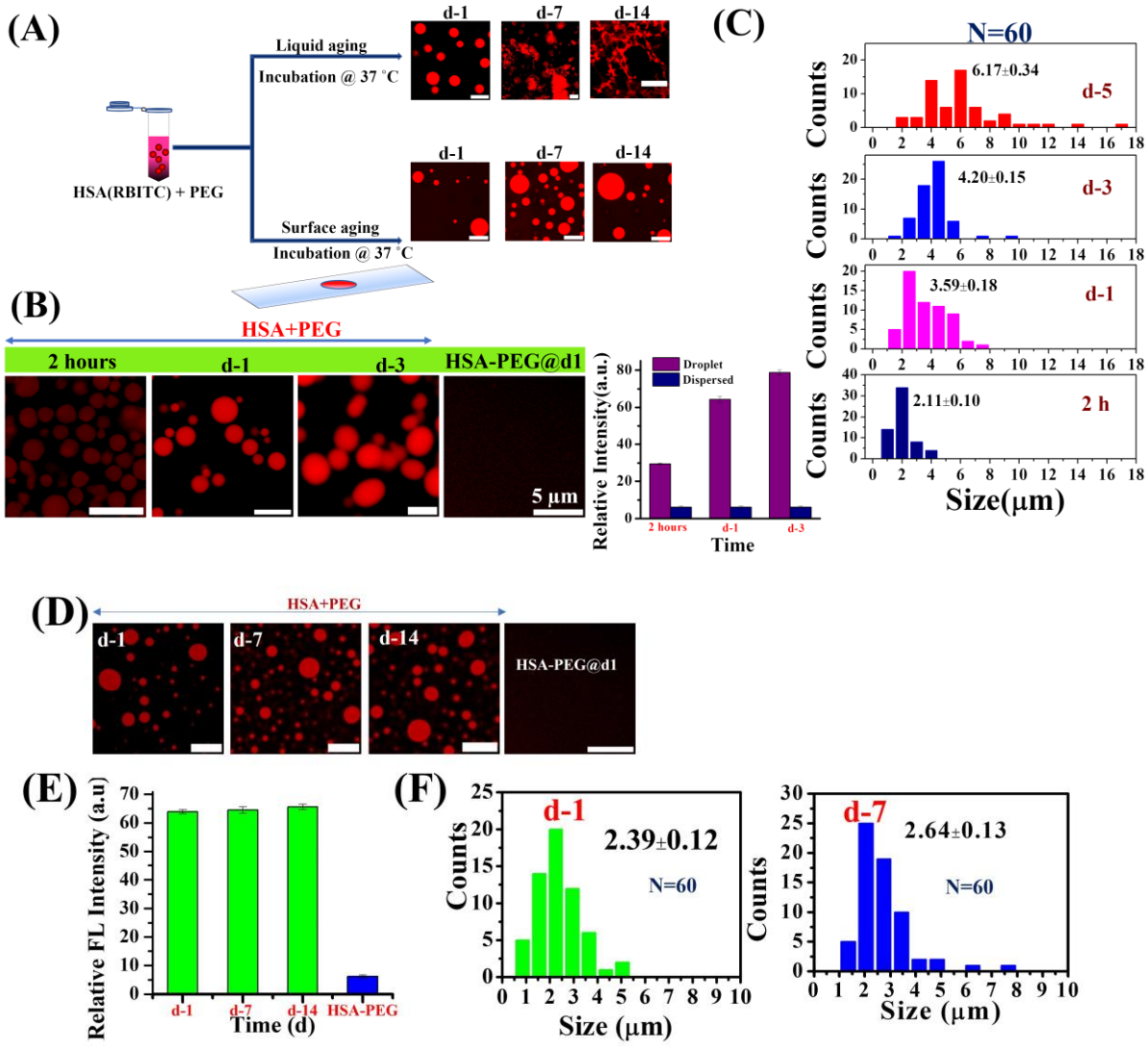

F

concentration determination inside the individual droplets using CLSM technique by comparing FL signal intensities between HSA (RBITC)+ PEG and HSA (RBITC) -PEG samples @ d1. (C) Size distribution histograms with time in liquid aging. (D, E) Protein concentration determination inside the individual droplets in surface aging by comparing the day wise samples FL signal intensities. (F) Size distribution histograms for surface aged samples. The data points represent the mean ± s.e.m. for three independent measurements for three (n = 3) independent experiments. All scale bars correspond to 5 μm.

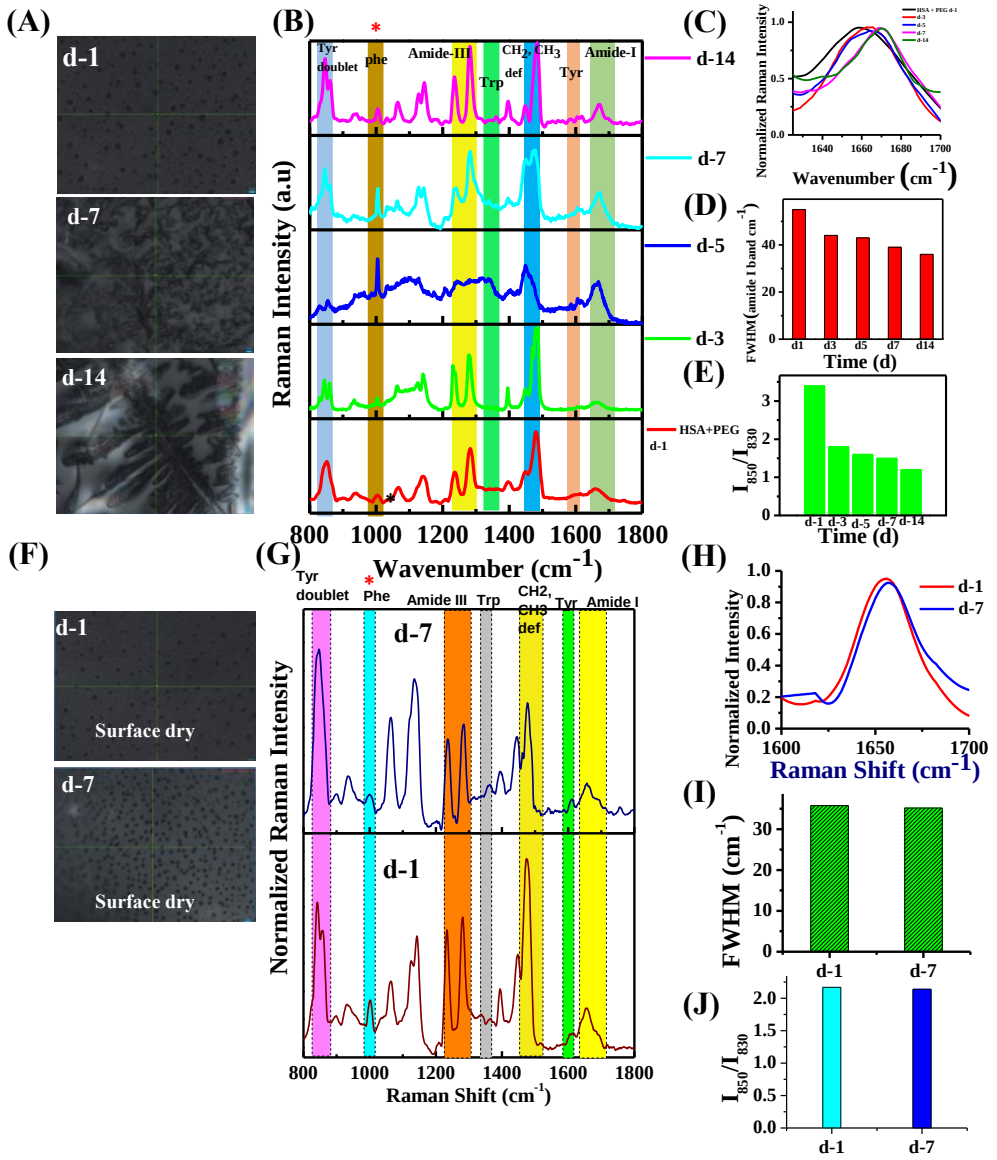

Figure 7. (A) Microscope images of d-1, d-7, d-14 were collected with Raman instrument set up to take spectra of individual droplets and fibril (B) Time-dependent individual Raman spectra (λ = 532 nm) of HSA+10% PEG of d-1, d-3, d-5, d-7 and d-14 on the glass slide. Spectra were normalized with Phenylalanine peak (red asterisk) at 1002 cm^{-1} for comparison. (C) Normalized Raman spectra of amide-I band of the HSA with the time. (D) FWHM (cm^{-1}) measurements of normalized amide I spectra of HSA+10% PEG with time (E) Tyrosine Fermi doublet (I_{850}/I_{830}) intensity comparison by bar diagram for the time-dependent HSA+10% PEG samples. (F) Microscope images were taken by Raman instrument set up for the surface dried samples at d-1 and d-7. (G) Time-dependent Raman spectra were recorded for the surface dried samples. Spectra were normalized at Phenylalanine peak (red asterisk) at 1002 cm^{-1} for

comparison. (H) Normalized Raman spectra of amide-I band for d-1 and d-7 samples. (I), (J) represent the FWHM (cm^{-1}) measurement and Tyrosine Fermi doublet (I_{850}/I_{830}) intensity comparison for surface dried samples respectively.

2.6. Raman spectra of the liquid phase and surface aged HSA sample with time

In addition, we analyzed the structural characteristics of HSA throughout the transformation from droplets to fibers in label-free manner by recording the Raman spectra of HSA+10% PEG samples over time. We conducted Raman spectroscopy on individual droplets using a laser with a wavelength of 532 nm. The Raman setup is used with a microscope to examine individual droplets and solid-aggregates **(Figure 7.A).** Our objective is to comprehend the structural alterations at the residue level during the stages of fibrillation in HSA. The spectra were adjusted by excluding the background signals originating from a 10% PEG solution. Both fibrils and droplets clearly display distinct Raman bands that correspond to various vibrational modes of the polypeptide chain of HSA. The Raman spectra of HSA is primarily characterized by the presence of amide I (1630-1670 cm^{-1}) and amide III (1230−1300 cm^{-1}) vibrations, as well as various vibrational modes of aromatic amino acids (tyrosine, tryptophan, and phenylalanine), and aliphatic side-chain vibrations **(Figure 7. B).** The amide I band is produced by the stretching of the carbonyl (−C=O) group, while the amide III band is principally caused by the stretching of the C−N bond and the bending vibrations of the N−H group in the polypeptide chain. The two distinctive bands observed in the Raman spectra are highly responsive to changes in the secondary structure of proteins and are commonly employed as markers for secondary structure analysis. Significantly, the amide I band of HSA droplets in liquid aging is observed at 1654 cm^{-1} on day 1 and undergoes a notable change in peak position after 14 days of incubation. The spectra are standardized to the phenylalanine peak at 1002 cm^{-1}. HSA in its natural form displays an amide band at 1654 cm^{-1}, which changes to 1665 cm^{-1} when solid-aggregate fibril was formed **(Figure 7. C).** This indicates a conversion from an α-helix structure to a β-sheet structure in the aggregated state of the HSA protein. In addition, we can see a reduction in the spread of the spectral lines by measuring the full width at half maximum, FWHM (cm^{-1}) of the amide-I band at 1654/1665 cm−1 in aggregates **(Figure 7.D)**. This suggests that there is less structural heterogenicity of HSA fibrillar aggregates compared to the droplet stage. The ratio of the intensities of the tyrosine Fermi doublet (I_{850}/I_{830}) in the Raman vibrational spectrum is an indicator of hydrogen bonding (H-bonding)

between the phenolic hydroxyl group of tyrosine and the water molecules in its vicinity. A typical value of ≥2.0 is observed for a tyrosine residue that is well-hydrated [27]. We noticed a decrease in the (I_{850}/I_{830}) value during the transition from droplets to fibril formation. The value in the droplets stage was approximately 3.4, and it subsequently fell to around 1.3 in the fibril aggregates **(Figure 7.E).** The ratio for fibrillar aggregates of HSA is considerably less than 2.0, indicating a lack of H-bonding interactions caused by dehydration and removal of interfacial water molecules from the hydrophobic fibrillar assembly of HSA. This theory is bolstered by previous research on proteins/peptides that create amyloid fibrils [28,29]. Previously, we showed by CLSM images that the droplets remained intact after a 14-day period of surface aging. We conducted time-dependent Raman spectroscopy on surface aged HSA+10% PEG samples, as shown in **(Figure 7 F, G).** An intriguing finding was made during the study. The spectral broadening of the amide I band **(Figure 7. H)** remained relatively constant until day 7, as indicated by the measurement of the FWHM (cm^{-1}) value **(Figure 7. I).** Additionally, the ratio of (I_{850}/I_{830}) remained almost unchanged (approximately 2.17 on day 1 and 2.14 on day 7) **(Figure 7. J)**. These observations suggest that, during surface aging, the droplet retained water molecules for an extended period of time. The ratio of (I_{850}/I_{830}) is higher than 2 for liquid-like droplets of HSA, indicating that the tyrosine residues of phase-separated HSA are more hydrated compared to the more structured fibrillar aggregates. Nevertheless, Raman vibrational modes of HSA expose the presence of a hydrated polypeptide chain with conformational heterogeneity inside the droplets and the hydration shells remain intact even after surface aging over a period of 14 days.

2.7. Modulatory role of ligands on the kinetics of liquid to solid-like phase transition

The impact of surfactant and metal ion on the transition of HSA from a liquid to a solid state was examined by the use of fluorescence microscopy, specifically confocal laser scanning microscopy (CLSM). The surfactant known as SDS has been observed to exhibit a high propensity for binding to HSA. Previous research has demonstrated that Sodium Dodecyl Sulfate (SDS) has the ability to safeguard HSA from thermal denaturation and gelation, as well as prevent aggregation within a certain concentration range [21]. Within a specified concentration range of sodium dodecyl sulfate (SDS), here we used 20 mM SDS to bind with HSA that exhibits the ability to maintain its helical structure and extend the duration of gel formation [22]. Furthermore, HSA remains in a liquid state for a period of up to 29 days, with the presence of small droplets were seen on @ d 1 day **(Figure 8. A)** The introduction of an anionic surfactant results in the generation of a negative charge on the surface of the HSA

protein, hence impeding aggregation and maintaining the protein in an unfolded conformation. Conversely, the introduction of $CuCl_2$ (250 μM) led to an elevation in the viscosity of the HSA solution, hence inducing alterations in the hydrogen bonding configuration. Furthermore, the Cu^{2+} ion effectively facilitates the structural conversion of HSA molecules from an α-helix conformation to a β-sheet conformation by diminishing the stability of disulfide bridges and initiating the unfolding of the α-helix structure. The presence of Cu^{2+} ions facilitate the aggregation of HSA molecules **(Figure 8. B)** due to the bridging and electrostatic shielding effects exerted by the Cu^{+2} ion [23].

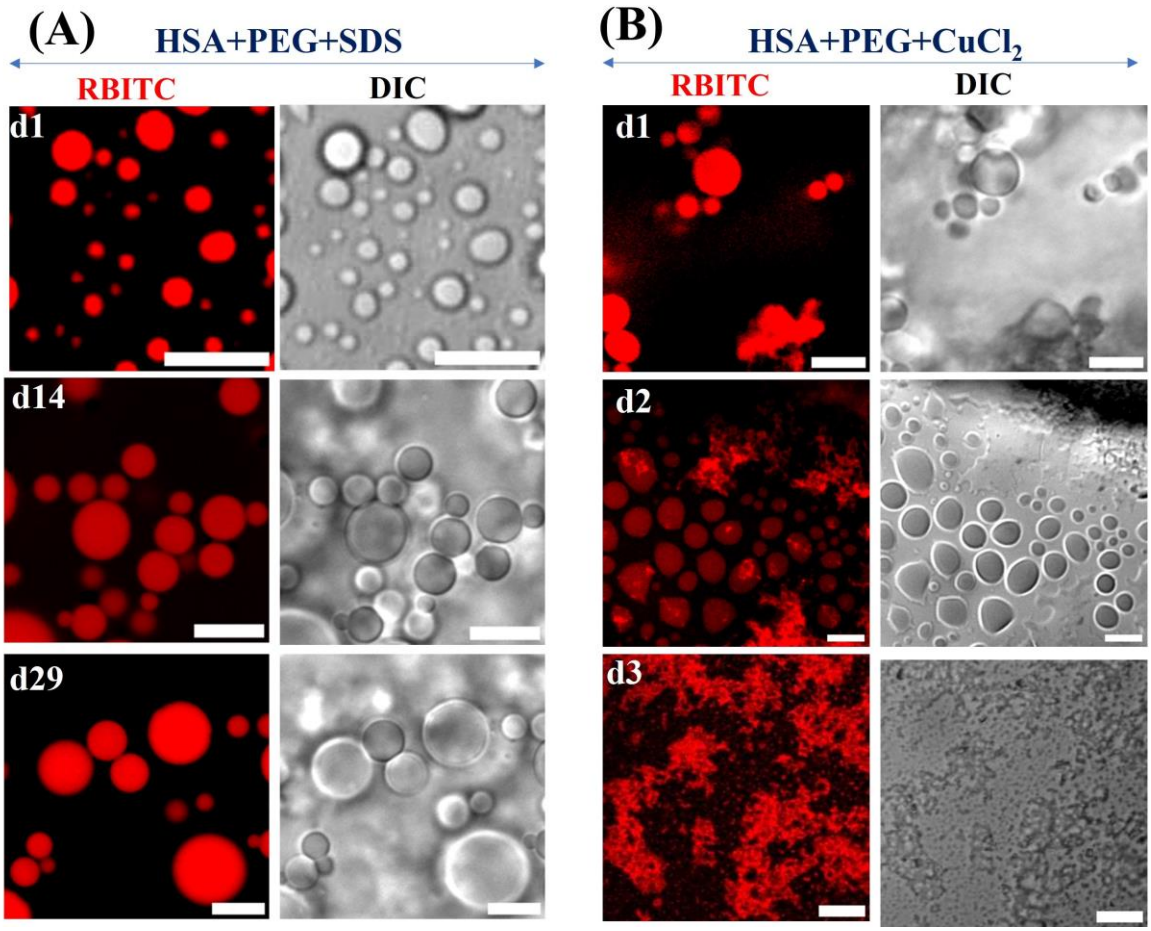

Figure 8. (A) Confocal images of HSA 500 μM bound with 20 mM SDS, in presence of PEG 10% at day 1 to day 29. (B) Confocal images of HSA+10% PEG with $CuCl_2$ (250 μM) at day 1 to day 3 and Solid aggregates like structure formed @ d 3.

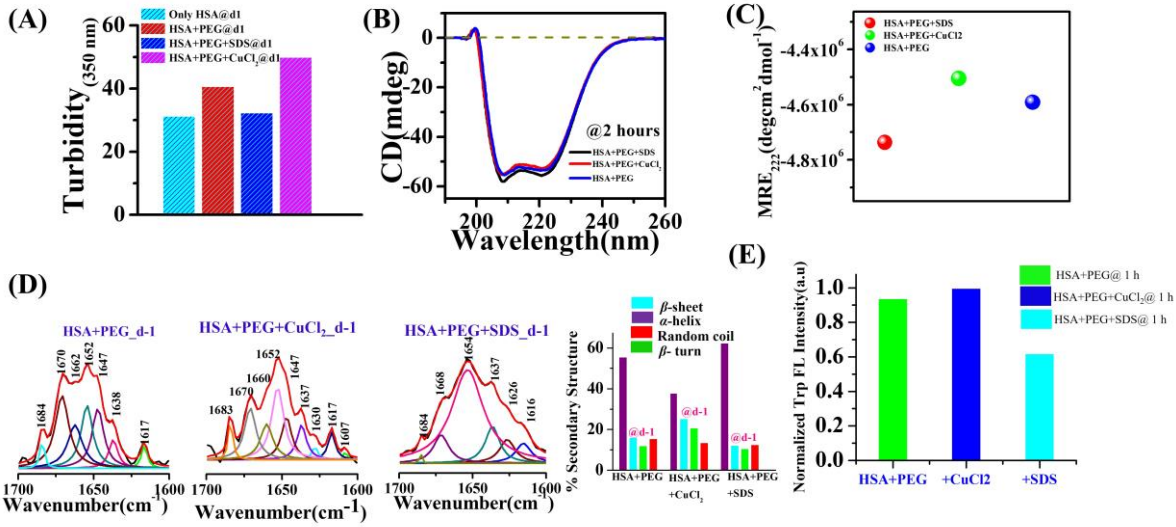

Figure 9. (A) Turbidity assay of ligand bound HSA @d-1. (B) Changes in the CD spectra, (C) MRE_{222} profile, Samples were diluted by 100-fold before spectral measurements. (D) Deconvoluted FTIR spectra of ligand bound HSA incubation at 37 °C of d-1, the bar diagram represents the percentage of secondary structures alternation in ligand bound study estimated from the deconvoluted FTIR spectra. (E) Normalized Tryptophan FL intensity profile of HSA+10% PEG in presence of ligands.

2.8. Analysis of secondary structures and conformational changes in the presence of ligands

Furthermore, we investigated the structural and conformational changes in presence of metal ion and surfactant. The intriguing results from the CLSM images of ligand bound study inferred the secondary and conformational changes. The turbidity profile **(Figure 9. A)** showed that the turbidity was maximum in presence of $CuCl_2$, and lowest when protein bound with SDS. It was direct evidence that the phase separation is faster in presence of $CuCl_2$ and that facilitated the droplets to fiber stage at day 3. On the other hand, the turbidity value in presence of SDS was much lower compare to only HSA+10% PEG. So, there should be changing in secondary structures of the protein. Therefore, we performed time-dependent CD spectra that revealed significant alteration in the secondary structures of HSA in presence of ligands, **(Figure 9. B)**. The calculated MRE_{222} values **(Figure 9. C)** of day 1 revealed that ellipticity at 222 upon decreased in presence of $CuCl_2$ (negative value decreased) and the value increased (negative value increased) in presence of SDS compare to HSA+10% PEG that inferred the compactness of HSA increases when it bound with SDS. The deconvoluted FTIR data **(Figure 9. D)** shows the % β-sheet structure was maximum in presence of $CuCl_2$ and lowest for SDS

case. So, Cu^{+2} enhance the β-sheet structures of HSA and this is the important factor for fast solid-like aggregation transition. In presence of SDS, droplets remained for over a long period of time due to the ability of SDS by maintaining HSA ellipticity and by prevention of α-helix to β-sheet structures conversion. Eventually, the conformational changes were largely altered in the presence of Cu^{+2} ion, that was confirmed from the Trp FL assay **(Figure 9. E).**

2.9. Surface aging phenomena of $CuCl_2$ bound HSA in presence of crowders

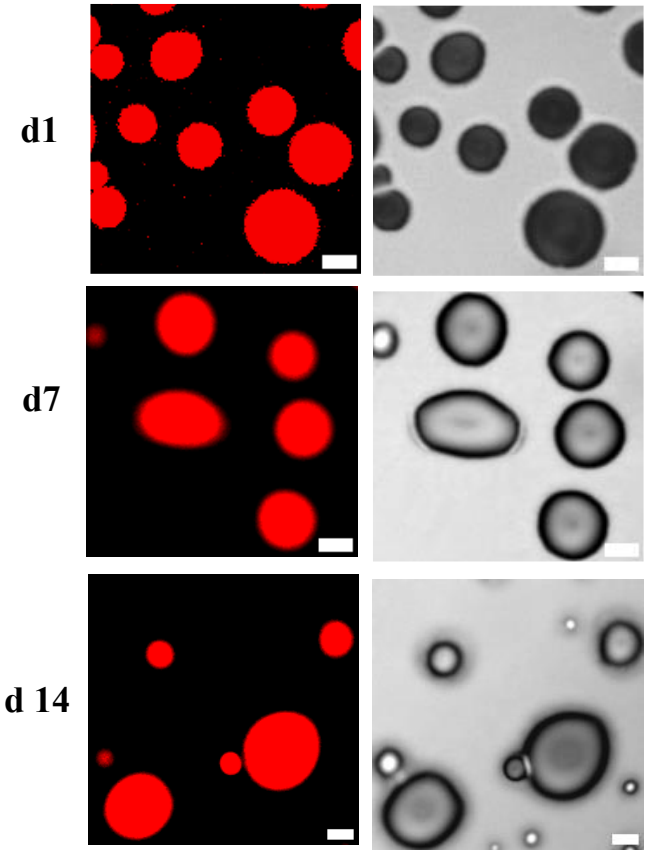

Figure 10. Surface aging phenomena of $CuCl_2$ bound HSA of day 1, day 7 and day 14 samples. All scale bars correspond to 5 μm.

We conducted additional research on the interaction between $CuCl_2$ and HSA in the presence of 10% PEG during surface aging. Specifically, we choose $CuCl_2$ bound to HSA because it accelerates the transition. We were intrigued to observe whether the liquid-to-solid transition occurred in the presence of Cu^{+2} during surface aging. We observed a fascinating outcome during the process of surface aging, where the droplets remained intact for a period of 14 days, no fibrillation was occurred. Hence, it is evident that the coalescence of droplets is a significant factor that promotes the formation of solid aggregates.

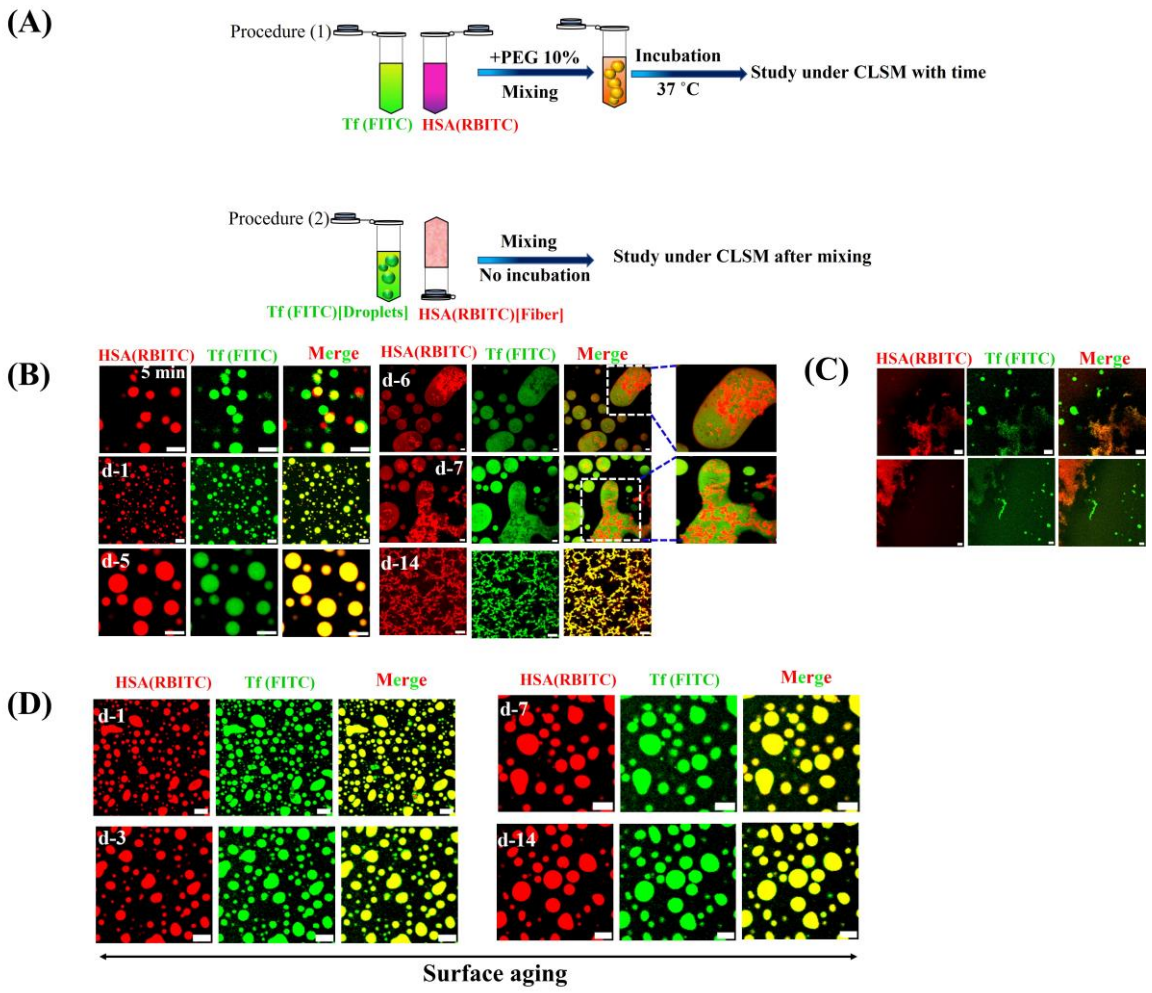

Figure 11. (A) Schematic representation of the procedure for phase separation study of HSA+ Tf in the same milieu under CLSM. (B) Time-dependent CLSM images of HSA+Tf in presence of 10% PEG by following the procedure (1). (C) CLSM images of HSA (fiber)+ Tf (droplets). (D) Surface aging CLSM images of HSA+Tf+ 10% PEG sample with time. Surace aged sample were incubated at 37 ºC.

2.10. Phase separation of HSA and Tf upon crowding in liquid phase and surface aging

Previous reports indicated that the in liquid phase the Tf droplets retained for approximately 21 days [1]. Therefore, we were interested in studying the phase behaviour phenomena of Tf condensates and HSA condensates in the same milieu. We followed two procedures to study this phase behaviour phenomenon under CLSM **(Figure 11. A)**. In the beginning of mixing two proteins (HSA [500 µM] tagged with RBITC and Tf [50 µM] tagged with FITC; for both the proteins [dye]:[Protein]= 1:1) with 10% PEG, droplets were formed. HSA had a pI of 4.7 and Tf had a pI of 6.7, due to this the droplets stuck together (see the

Merge image of 5 minutes of mixing, which shows a yellow signal due to the merging of HSA and Tf droplets along with the individual red and green signals). However, as the incubation time progressed, the HSA and Tf droplets coalesced into fiber on day 14. Notably, the CLSM images revealed solid-aggregate-like structures inside the droplets on days 6 and 7 was for HSA aggregation, not Tf, causing the intense red signal in merge CLSM images. The kinetics of Tf droplet aggregation are likely slow. We need to further investigate whether the Tf droplets actually underwent aggregation, or if the proteins were deposited due to their different isoelectric points. Interestingly, our skeptical investigation (procedure 2) suggested that Tf did not undergo aggregation in the presence of HSA. A different pI value led to the deposition of Tf over HSA. **Figure 11. C** illustrates the presence of Tf droplets in addition to HSA fiber during the initial mixing of HSA fiber and Tf droplets. Without incubation, the long-retained Tf droplets were unable to fibrillate. Therefore, we confirmed that the Tf droplets deposited to the HSA. If we only observed Tf droplets, we could deduce that Tf follows the same fibrillation pathway as HSA, in the presence of crowders and HSA. Next, we studied the surface-aged behaviour of HSA and Tf droplets **(Figure 11.D).** The droplets sustained over a long period of time around day 14 due to the absence of simultaneous fusion of droplets and water retention inside the droplets. (**See Figure 7. G.** for the surface-aged Raman study section.)

Chapter 3

Conclusion

3. Conclusion

We have discovered the intriguing phase behavior of HSA in presence of metal ion and surfactant. Cu^{+2} facilitated faster liquid to solid-like aggregation whether SDS prevent the transition. We showed the fibrillation pathway of HSA that how protofibril like aggregated structure originates then this aggregates like structures formed complete fiber structures. AFM image analysis indicates the height of the droplets decreases during the transition and at fiber stage the height is minimum. The protein fibrillation is due to the conversion of α-helix to β-sheet structures that we conclude from CD-spectra and deconvoluted FTIR data measurements. The liquid phase and surface aging observations astonished us. The HSA droplets sustained over a long period of time in surface aging. We conclude the reason behind this phenomenon by estimating approximate protein concentration determination, droplets Size distribution and most importantly by Raman spectrum. Raman shows that the droplet to fiber transition is due to expulsion of water molecules from droplets. We showed that how two mixtures of proteins i.e., HSA and Tf undergo phase separation upon crowding in the same milieu. The long sustained Tf droplets undergo fibrillation in the presence of HSA in liquid phase study but later we concluded from CLSM images that due to their different pI value they had just deposited over. We have successfully found the reason behind fibrillation, that the coalescence of droplets is a significant factor that promotes the formation of solid aggregates, why the fibrillation step is faster in liquid phase aging, how ligands effect the HSA phase separation, the mechanistic insight of fibrillation and the liquid phase, surface aging of HSA and Tf upon crowding in the same milieu.

Chapter 4

References

4.1. References

[1] Patel, C.K; Rani, C.; Kumar, R.; Mukherjee, T. K. Macromolecular Crowding Promotes Re-Entrant Liquid–Liquid Phase Separation of Human Serum Transferrin and Prevents Surface-Induced Fibrillation. *J. Biol. Macromol.* **2023**, *24*, 3917–3928.

[2] Roos, A.; Boron, W. F. Intracellular PH. *Physiol. Rev.* **1981**, *61*, 296–434.

[3] Ponsoda, J.M.; Díaz, A. Positive Emotions in Family Caregivers of Alzheimer's Disease Patients: Factors Associated with Gain in Caregiving from a Gender Perspective. *J. Clin. Med.* **2024**, *13*, 2322.

[4] Halloway, S.; Wagner, M.; Tangney, C.; Lange-Maia, B. S.; Bennett, D. A.; Arvanitakis, Z.; Schoeny, M. Profiles of Lifestyle Health Behaviors and Cognitive Decline in Older Adults. *Alzheimers Dement.* **2023**.

[5] Horvath, I.; Weise, C. F.; Andersson, E. K.; Chorell, E.; Sellstedt, M.; Bengtsson, C.; Olofsson, A.; Hultgren, S. J.; Chapman, M.; Wolf-Watz, M.; Almqvist, F.; Wittung-Stafshede, P. Mechanisms of Protein Oligomerization: Inhibitor of Functional Amyloids Templates α-Synuclein Fibrillation. *J. Am. Chem. Soc.* **2012**, *134*, 3439–3444.

[6] Breydo, L.; Uversky, V. N. Molecular Mechanisms of Protein Misfolding. *Bio-nanoimaging* **2014**, 1–14.

[6] Iadanza, M. G.; Jackson, M. P.; Hewitt, E. W.; Ranson, N. A.; Radford, S. E. A New Era for Understanding Amyloid Structures and Disease. *Nat. Rev. Mol. Cell Biol.* **2018**, *19*, 755–773.

[7] Dogra, P.; Joshi, A.; Majumdar, A.; Mukhopadhyay, S. Intermolecular Charge-Transfer Modulates Liquid–Liquid Phase Separation and Liquid-To-Solid Maturation of an Intrinsically Disordered PH-Responsive Domain. *J. Am. Chem. Soc.* **2019**, *141*, 20380–20389.

[8] Patel, C. K.; Singh, S.; Saini, B.; Mukherjee, T. K. Macromolecular Crowding-Induced Unusual Liquid–Liquid Phase Separation of Human Serum Albumin via Soft Protein–Protein Interactions. *J. Phys. Chem. Lett.* **2022**, *13*, 3636–3644.

[9] Bhattacharya, A.; Prajapati, R.; Chatterjee, S.; Tushar Kanti Mukherjee. Concentration-Dependent Reversible Self-Oligomerization of Serum Albumins through Intermolecular *β*-Sheet Formation. *Langmuir*. **2014**, *30*, 14894–14904

[10] Yuan, C.; Levin, A.; Chen, W.; Xing, R.; Zou, Q.; Herling, T. W.; Pavan Kumar Challa; Knowles, J.; Yan, X. Nucleation and Growth of Amino Acid and Peptide Supramolecular Polymers through Liquid–Liquid Phase Separation. *Angew. Chem.* **2019**, *58*, 18116–18123.

[11] Ray, S.; Singh, N.; Kumar, R.; Patel, K.; Pandey, S.; Datta, D.; Mahato, J.; Panigrahi, R.; Navalkar, A.; Mehra, S.; Gadhe, L.; Chatterjee, D.; Sawner, A. S.; Maiti, S.; Bhatia, S.; Gerez, J. A.; Chowdhury, A.; Kumar, A.; Padinhateeri, R.; Riek, R. α-Synuclein Aggregation Nucleates through Liquid–Liquid Phase Separation. *Nat. Chem.* **2020**, *12*, 705–716.

[12] Maier, R.; Fries, M. R.; Buchholz, C.; Zhang, F.; Schreiber, F. Human versus Bovine Serum Albumin: A Subtle Difference in Hydrophobicity Leads to Large Differences in Bulk and Interface Behavior. *Cryst. Growth Des.* **2021**, *21*, 5451–5459.

[13] Mandeville, J. S.; Tajmir-Riahi, H. A. Complexes of Dendrimers with Bovine Serum Albumin. *J. Biol. Macromol.* **2010**, *11*, 465–472.

[14] Domínguez, M.; Cortés-Figueroa, J. E.; Meléndez, E. Biological Interaction of Molybdenocene Dichloride with Bovine Serum Albumin Using Fluorescence Spectroscopy. *J. Chem. Educ.* **2017**, *95*, 152–157

[15] Wu, H.; Fuxreiter, M. The Structure and Dynamics of HigherOrder Assemblies: Amyloids, Signalosomes, and Granules. *Cell.* **2016**, 165, 1055−1066.

[16] Anderson, N. L.; Anderson, N. G. The Human Plasma Proteome: History, Character, and Diagnostic Prospects. *Mol Cell Proteomics.* **2002**, *1***,** 845–867.

[17] Sarkar, M.; Lu, J.; Pielak, G. J. Protein Crowder Charge and Protein Stability. *Biochemistry* **2014**, 53, 1601−1606.

[18] Patel, A.; Lee, Hyun O.; Jawerth, L.; Maharana, S.; Jahnel, M.; Hein, Marco Y.; Stoynov, S.; Mahamid, J.; Saha, S.; Franzmann, Titus M.; Pozniakovski, A.; Poser, I.; Maghelli, N.; Royer, Loic A.; Weigert, M.; Myers, Eugene W.; Grill, S.; Drechsel, D.; Hyman, Anthony A.; Alberti, S. A Liquid-To-Solid Phase Transition of the ALS Protein FUS Accelerated by Disease Mutation. *Cell.* **2015**, *162*, 1066–1077.

[19] Arora, S. L.; Debsankar Saha Roy; Sukumar Maiti; Rama, S. Phase Separation and Aggregation of a Globular Folded Protein Small Ubiquitin-like Modifier 1 (SUMO1). *J. Phys. Chem. Lett.* **2023**, *14*, 9060–9068.

[20] Mishra, P. P.; Bhatnagar, J.; Datta, A. The Interplay of Hydrophobic and Electrostatic Effects in the Surfactant-Induced Aggregation/Deaggregation of Chlorin P_6. *J. Phys. Chem.* **2005**, *109*, 24225–24230.

[21] Turro, N. J.; Lei, X.-G.; Ananthapadmanabhan, K. P.; Aronson, M. Spectroscopic Probe Analysis of Protein-Surfactant Interactions: The BSA/SDS System. *Langmuir*. **1995**, *11*, 2525–2533.

[22] Nnyigide, O. S.; Hyun, K. The Protection of Bovine Serum Albumin against Thermal Denaturation and Gelation by Sodium Dodecyl Sulfate Studied by Rheology and Molecular Dynamics Simulation. *Food Hydrocoll.* **2020**, *103*, 105656.

[23] Jing, P. P.; Li, Y. X.; Su, Y. H.; Liang, W. L.; Leng, Y. X. The Role of Metal Ions in the Behavior of Bovine Serum Albumin Molecules under Physiological Environment. *Spectrochim Acta A Mol Biomol Spectrosc.* **2022**, *267*, 120604.

[24] Wegmann, S.; Eftekharzadeh, B.; Tepper, K.; Zoltowska, K. M.; Bennett, R. E.; Dujardin, S.; Laskowski, P. R.; MacKenzie, D.; Kamath, T.; Commins, C.; Vanderburg, C.; Roe, A. D.; Fan, Z.; Molliex, A. M.; Hernandez-Vega, A.; Muller, D.; Hyman, A. A.; Mandelkow, E.; Taylor, J. P.; Hyman, B. T. Tau Protein Liquid–Liquid Phase Separation Can Initiate Tau Aggregation. *EMBO J.* **2018**, *37*. No. e98049.

[25] Williams, A. D.; Sega, M.; Chen, M.; Kheterpal, I.; Geva, M.; Berthelier, V.; Kaleta, D. T.; Cook, K. D.; Wetzel, R. Structural Properties of Aβ Protofibrils Stabilized by a Small Molecule. *Proc Natl Acad Sci U S A.* **2005**, *102*, 7115–7120.

[26] Ambadipudi, S.; Reddy, J. G.; Biernat, J.; Mandelkow, E.; Zweckstetter, M. Residue-Specific Identification of Phase Separation Hot Spots of Alzheimer's-Related Protein Tau. *Chem. Sci.* **2019**, *10*, 6503–6507.

[27] Avni, A.; Joshi, A.; Walimbe, A.; Pattanashetty, S. G.; Mukhopadhyay, S. Single-Droplet Surface-Enhanced Raman Scattering Decodes the Molecular Determinants of Liquid-Liquid Phase Separation. *Nat. Commun.* **2022**, 13, 4378.

[28] Balbirnie, M.; Grothe, R.; Eisenberg, D. S. An Amyloid Forming Peptide from the Yeast Prion Sup35 Reveals a Dehydrated β-Sheet Structure for Amyloid. *Proc. Natl. Acad. Sci. U. S. A.* **2001**, 98, 2375−2380.

[29] Tarus, B.; Straub, J. E.; Thirumalai, D. Probing the Initial Stage of Aggregation of the Abeta (10−35) −Protein: Assessing the Propensity for Peptide Dimerization. *J. Mol. Biol.* **2005**, 345, 1141− 1156.

4.2. Supporting Information

1. Materials

Human Serum Albumin, Polyethylene glycol 8000 (PEG 8000), rhodamine B isothiocyanate (RBITC), fluorescein-5-isothiocyanate (FITC), , hellmanex III and the Pur-A-Lyzert dialysis kit (molecular weight cutoff 3.5 kDa) were purchased from sigma-Aldrich. Sodium dihydrogen phosphate monohydrate ($NaH_2PO_4.H_2O$), di-sodium hydrogen phosphate heptahydrate ($Na_2HPO_4.7H_2O$), Copper Chloride ($CuCl_2$), Sodium dodecyl sulphate (SDS), sodium azide (NaN_3), sodium chloride (NaCl), and ethanol (EtOH) were purchased from Merck. All the chemicals were used without any further purification. Eco Testr pH1 pH meter was used to adjust the final pH (± 0.1) of all the buffer solutions. Milli-Q water was obtained from a Millipore water purifier system (Milli-Q integral).

2. Methods

2.1. Prediction of LCDs and IDRs of HSA

To predict the low complexity domains (LCDs) and disorder regions (IDRs) in HSA, we used Simple Molecular Architecture Research Tool (SMART) (http://smart.embl-heidelberg.de/) and IUPred2 (https://iupred2a.elte.hu/) respectively.[1,2]

2.2. Preparation of Buffer Solution and Crowder Solution

Buffer solution with pH values of 7.4(Phosphate buffer saline) was prepared by using Milli-Q water. phosphate buffer (pH 7.4, 0.02% sodium azide), in the presence of 50 mM NaCl. All the buffer solutions were kept in the hood under sterile condition.

10% (w/v) PEG 10% is (prepared from a stock solution of 40% (w/v) PEG 8000.

2.3. Labelling of Protein and Crowders with Fluorescent Dyes

The concentration of HSA was estimated spectrophotometrically using the reported extinction coefficient of 43,824M-1 cm-1 M^{-1} cm^{-1} at λ = 280 nm. HSA was labelled with RBITC dye according to an earlier reported method.[1] In short, 3 mM HSA was mixed with RBITC in a molar ratio of 1:1 ([HSA]: [RBITC]). The mixture was incubated for 4 h at room temperature followed by 6 h at 4 ℃ on a magnetic stirrer with slow rotation. After the completion of the reaction, the unconjugated dyes were removed using dialysis (molecular weight cut-off 3.5 kDa) against 10 mM PBS at 4 ℃ for 12 h with regular buffer exchange in 2 h intervals.

2.4. Sample preparation:

Liquid ageing; For the ageing of the samples in liquid medium, we prepared HSA in Phosphate buffer saline (PBS; pH 7.4) in the presence of PEG 10% and kept these solutions in 37 °C incubation chamber. For their characterisation in confocal microscopy, we drop casted the liquid sample on the glass surface and then covered with a coverslip making it sandwich and sealed them with nail paint to avoid evaporation. The stock solution of $CuCl_2$, and SDS solution were prepared in PBS for ligand bound study.

2.5. LLPS Assay of HSA in the Presence of PEG 8000:

LLPS at pH 7.4 was examined by equilibrated 500 μM HSA with 10% (w/v) PEG 8000 in different buffer solutions at different time intervals. The samples were prepared in 5 mL glass vials and kept for incubation at 37˚C inside a constant temperature incubator.

To check the time dependent LLPS behaviour of HSA. For all measurements, droplet formation was confirmed by CLSM and FESEM.

2.6. ThT Binding Assay

Stock solution of 2 mM ThT was prepared in pH 7.4 PBS. 20 µM ThT was used for the study of ThT binding assay. The ThT binding assay of HSA was carried out by Horiba FluoroMax Fluorometer using the excitation laser 450 and emission in the range of 490-550 nm.

2.7. Calculation of Student *t*-test

The independent experiment values were plotted in n Microsoft excel and putting the T-test formula. Statistical significance was assessed by a two-tailed, unpaired Student's t-test with ***, P value < 0.001; **, P value < 0.01; and not significant (NS), P > 0.05.

2.8. Protein concentration determination inside the droplets

We estimated the concentration of HSA inside the droplet (dense) phase and dispersed (light) phase by using HSA-RBITC (Protein : dye = 1:1). The fluorescence intensity of droplets was compared against the FL intensity of HSA(RBITC)-PEG at day 1 sample by *Image J* software. The mean (n = 40 droplets) estimated concentration was increasing day-wise. We estimated the concentration up to day 5 as at solid aggregation structures were formed start from day 6. In the dispersed phase the concentration was ~500 µM and the concentration inside the droplets increased around 10-12 folds. This is an approximate concentration estimation. Data are represented as mean ± SEM of three independent measurements.

2.9. Surface aging

For surface aging experiments, 20 µL aliquot of HSA+10% PEG sample (500 µM HSA in phosphate buffer) were drop-cast over a cleaned glass slide and kept inside the incubation chamber at 37 °C for 1- to 14-days for studied under CLSM as well for Raman spectroscopy.

2.10. Ligand bound study: Sample preparation

Stock solution of $CuCl_2$ and SDS were prepared in PBS (pH 7.4). For liquid aging study we used 250 µM $CuCl_2$ and 20 mM SDS and then mixed with HSA 500 µM in PBS then we added 10 % PEG.

3. Characterization Techniques

3.1. Confocal Laser Scanning Microscopy (CLSM)

The confocal images were obtained using an inverted confocal microscope, Olympus fluoView (model FV1200MPE, IX-83) through an oil immersion objective (100×1.4 NA). The samples were excited using two different diode lasers (488 and 559 nm) by using appropriate dichroic and emission filters in the optical path. For clear imaging of the droplets, 10-15 µL aliquot of the sample solution was drop cast on a cleaned glass slide followed by washing with milli-Q to wash away the extra crowder and then covered with a cover slip. The prepared samples were placed in a desiccator under vacuum for 10 minutes.

3.2. Fourier-Transform Infrared (FTIR) Spectroscopy

FTIR spectroscopy was performed to determine the secondary structure of the proteins using a Bruker spectrometer (Tensor-27)**.** 10 µL of liquid sample of 500 μM HSA in the presence of PEG 8000 in PBS pH 7.4 buffer were used for FTIR measurement. The spectra were recorded in the range of 4000–400 cm^{-1}. Fourier self-deconvolution (FSD) method was used to deconvolute the spectra corresponding to the wavenumbers 1700−1600 cm^{-1}.[2]The Lorentzian curve fitting was done to fit the spectra using origin 8.1 software. The experiments were performed twice with similar observations.

3.3 UV−vis Spectroscopy

Absorption spectra were recorded in a quartz cuvette (1 cm × 1 cm) using a Varian Carry 100 Bio UV−visible spectrophotometer.

3.4. Fluorescence Spectroscopy

The fluorescence spectra were recorded in a quartz cuvette (1 cm × 1 cm) using a HORIBA Jobin Yvon, model FM-100 Fluoromax-4 Spectrofluorometer at constant temperature 37 ºC. The slit width was kept at 3 nm.

3.5. Circular Dichroism (CD) Spectroscopy

CD spectra were recorded on a JASCO J-815 CD spectropolarimeter using a quartz cell of 1 mm path length with a scan range of 190-260 nm. Scans were recorded with a slit width of 1 mm and speed of 50 nm/min. For CD measurements, 500 μM HSA solutions were diluted by 100-fold to make the final effective concentration of 5 μM. The mean residue ellipticity (MRE) in deg cm2 dmol-1 of HSA at 222 nm was calculated using the formula,

MRE = $\theta_{obs}(mdeg)M\ /nlc$ where Θ_{obs} is the CD in millidegrees, M is the molecular weight of the protein in g dmol-1, n is the number of amino acid residues (585 in the case of HSA), l is the path length (0.1 cm) of the cuvette and c is the concentration of the protein in gL -1

3.6. Raman spectroscopy

For all Raman measurements, the dense phase from reaction mixtures was used. The resuspended dense phase was deposited onto a glass slide covered with an aluminum sheet and half-dried. An inVia laser Raman microscope (HORIBA) was used for recording all the spectra. The sample was focused using a 100x objective lens (Nikon, Japan), and a 532-nm NIR laser was used for excitation, with an exposure time of 10 s and 500 mW laser power. Spectra were recorded for HSA+10% PEG droplets at different time points. The instrument's in-built Wire 3.4 software was used for data acquisition. All the data were averaged over 10 scans. Acquired spectra were baseline corrected and smoothened using Wire 3.4. Spectra were plotted using Origin 2018b.

3.7. Atomic Force Microscopy

AFM images were acquired using an PERK atomic force microscope operating in tapping mode. For sample preparation, 10 μL aliquots were taken from incubated samples and deposited on freshly cleaved, Milli-Q water washed muscovite mica (Grade V-4 mica from SPI, PA). XEI software was used for image processing. The height profiles were analysed from XEI.

3.8. Rheological Behaviour of the Hydrogel

Viscoelastic characterization of the HSA gel was carried out by rheology. Anton Paar Physica rheometer (model no MCR 301) was used for all rheological experiments. The linear viscoelastic region (LVR) of the synthesized hydrogel was determined by the amplitude sweep experiment at a constant frequency of 10 rad/s. Hydrogel was placed on the rheometer disc by using a micropipette. A parallel plate with a diameter of 25 mm was used for this experiment. The TruGap was set at 0.5 mm. The mechanical strengths of the hydrogels were determined by frequency sweep experiment. In the frequency sweep experiment, the storage modulus (G') and loss modulus (G") were plotted as a function of frequency. The range of frequency was 0.1–100 rad s–1.

References of Supporting Information

1) James, N. G.; Mason, A. B. Protocol to Determine Accurate Absorption Coefficients for Iron-Containing Transferrins. *Anal. Biochem.* **2008**, *378*, 202–207.

2) Yang, H.; Yang, S.; Kong, J.; Dong, A.; Yu, S. Obtaining Information about Protein Secondary Structures in Aqueous Solution Using Fourier Transform IR Spectroscopy. *Nat. Protoc.* **2015**, *10*, 382–396.